Proceedings of the ASME 2010 3rd Joint US-European Fluids Engineering Summer Meeting and 8th International Conference on Nanochannels, Microchannels, and Minichannels
FEDSM-ICNMM2010
August 1-5, 2010, Montreal, Canada

FEDSM-ICNMM2010-30548

COHERENT STRUCTURES IN THE NEAR WAKE OF A BLUNT TRAILING EDGE PROFILED BODY

Lakshmana Sampat Doddipatla
Graduate Research Assistant,
The Boundary Layer Wind Tunnel Laboratory,
The University of Western Ontario
London, ON, Canada
sdoddipa@uwo.ca

Arash Naghib-Lahouthi
Graduate Research Assistant,
The Boundary Layer Wind Tunnel Laboratory,
The University of Western Ontario
London, ON, Canada
anaghibl@uwo.ca

Horia Hangan
Professor and Director,
The Boundary Layer Wind Tunnel Laboratory,
The University of Western Ontario
London, ON, Canada
hmh@blwtl.uwo.ca

Kamran Sidiqqui
Associate Professor,
Department of Mechanical and Materials Engg.,
The University of Western Ontario
London, ON, Canada
ksiddiqui@eng.uwo.ca

ABSTRACT

Wake flows behind two dimensional bodies are mainly dominated by two coherent structures, namely the Karman-Benard vortices and the streamwise vortices, also referred to as rolls and ribs respectively. The three dimensional wake instabilities lead to distinct instability modes (mode-A, mode-B and mode-C or mode-S) depending on the flow Reynolds number and geometric shape. The present investigation explores the mechanism in which the flow transitions to three dimensionality in the near wake of a profiled leading edge and blunt trailing edge body. A combination of Planar Laser Induced Fluorescence visualizations and Particle Image Velcoimetry measurements are conducted in the Reynolds numbers ranging from 250 to 550. The results indicate that three instability modes (mode-A, mode-B and mode-C) appear in the wake transition to three dimensionality, and their order of appearance does not occur through the traditional route as observed in circular cylinder flows. It is found that mode-C instability with a spanwise spacing of 2.4D dominates the near wake development.

Keywords: Wake instabilities, Wake transition, PLIF, PIV, POD

1. INTRODUCTION

Wake flows behind two dimensional bodies are mainly dominated by two coherent structures, i.e. the Karman-Benard vortices and the streamwise vortices, also referred to as rolls and ribs respectively. It is known that Karman vortex shedding in the wake causes an increase in the mean drag and lift fluctuations on the body. It has been established that ribs wrap around rolls and are interconnected [1]. The transition to turbulence is thought to determine the mixing properties, and further more the combined development of both two and three dimensional instabilities and their receptivity to various forcing and actuation techniques is believed to play a dominant role in control strategies to mitigate vortex shedding and minimize drag [2 to 6]. Identifying the most unstable secondary wake instabilities and triggering them would be the most efficient way to develop a wake control mechanism. This work focuses on identifying the spacing of the of the most unstable streamwise wake instability using PLIF (Planar Laser Induced Fluorescence) and PIV (Particle Image Velcoitmetry) measurements in the near wake of a blunt trailing edge profiled body, and by application of Proper Orthogonal Decomposition (POD) to the PIV data. We choose to study the flat plate geometry with profiled leading edge and blunt trailing, as it provides the desired upstream boundary layer velocity profile at

the trailing edge without the uncontrollable effects of forced separation-reattachment associated with sharp corners of a square leading edge.

The near wake of a two dimensional body is very critical due to dominant instability in the flow, i.e. the primary two dimensional instability that leads to the vortex street formation (Unal and Rockwell [7], Monkewitz [8]). For circular cylinder this bifurcation occurs at critical Reynolds number (Re_c) $\approx$45. Further transition in the near wake is responsible for the formation of three dimensional secondary instabilities that leads to turbulent state as found in the experimental work of Williamson [9], Hammache and Gharib [10], Eisenlohr and Ekelmann [11], and numerical work of Barkley and Henderson [12]. Their works suggest that the transition from two to three dimensional instabilities occur in a wide range of Reynolds numbers from Re_c $\approx$140 to $\approx$190. The possible reason is attributed to the background disturbances influencing the critical Reynolds number (Re_c) (Unal and Rockwell [7]). However, other factors such as aspect ratio (height to spanwise length), the end conditions and even shedding modes e.g. parallel or oblique can influence Re_c (Prasad and Williamson [13]). For circular cylinder flows, Williamson [9] demonstrated that two distinct three dimensional streamwise instability modes occur, i.e. mode-A and mode-B, depending on the flow Reynolds numbers. Mode-A occurs at Re_D>180 and is gradually replaced by mode-B at Re_D>230, and both modes coexist at Re_D=220. The spanwise spacing between streamwise vortices of Mode-A is scattered between 3D to 5D [9], but for Mode-B it has been demonstrated consistently to be around 1D [9] in various experiments for various Reynolds numbers. The spatio-temporal symmetry of mode-A and mode- B are shown in figure 1.

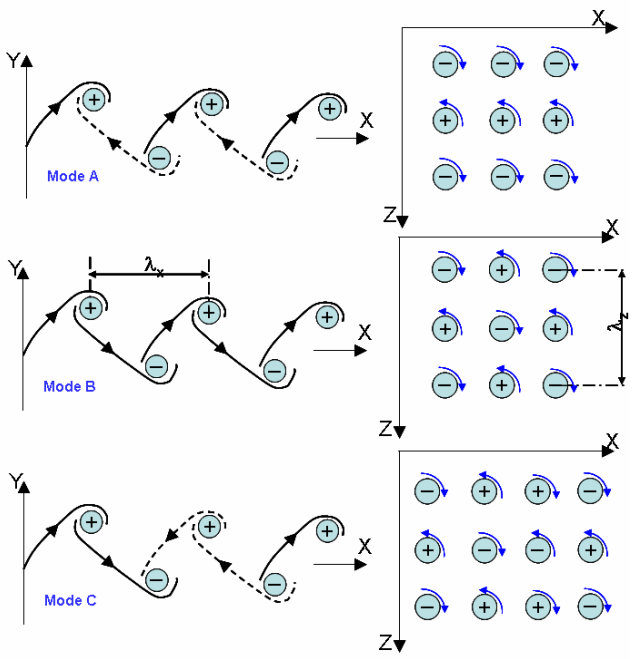

Figure 1. Description of Mode-A, Mode-B and Mode-C structures in XY and XZ planes

The major difference between the two modes is, for mode-A the regions of positive and negative vorticity alternate in the spanwise direction and with time. The sign of vorticity and there by direction of the secondary vortices, alternates twice every Karman cycle. For mode-B the vorticity pattern shows spanwise periodicity. Yet in contrast to mode-A, the sense of rotation does not change with time for a given spanwise location. Furthermore, the secondary vortices of the mode-B seem to be persistent in time and remain connected over many Karman cycles. The entire patterns of secondary vortices oscillate up and down sinusoidally during each cycle of Karman vortex formation. Zhang et al. [14] show that a third mode (mode-C) appears in the presence of an interference wire placed close to and parallel to the cylinder axis, with a spanwise wavelength of 2.0 cylinder diameters. For this mode, the vorticity direction of streamwise vortices connecting the spanwise vortices alternates every Karman vortex cycle at a particular spanwise location with time (figure 1). However, the full Floquet stability analysis of an unforced cylinder wake by Barkley and Henderson [12] captures only mode-A and mode-B instabilities. Hence it can inferred that possibility of other three dimensional instabilities can be excited which are stable under normal conditions, with suitable forcing.

Robichaux et al. [15] conducted low Re_D numerical simulation based on Floquet analysis and found same natural modes with larger spanwise spacing of 5.22D for Mode-A and 1.2D for Mode-B. Their model also predicted a third instability mode, which they denoted it by mode S with a spanwise spacing of 2.8D. This mode has the same features as mode-C as observed by Zhang et al. [14]; however this mode naturally evolved in the flow without any external forcing, compared to mode-C as in the case of circular cylinder. Robichaux et al. [15] found that mode S was subharmonic, with periodic double of the base flow. However Blackburn and Lopez [16] demonstrated that it is not true subharmonic, but repeats every second cycle.

Till here it appears that the wake of two-dimensional bluff bodies undergo transition to three dimensional flow and eventually turbulence, through the same sequence of transition as observed for circular cylinder [9] and that mode-B dominate the flow after a certain transition Reynolds number. Previous studies on square cylinder [15, 17, 18, 19], support this assumption, with a slight variation in the spanwise spacing of these instabilities. However, Ryan et al. [20] numerically investigated the near wake structure of a flat plate body with elliptical leading edge and blunt trailing edge for various aspect ratios (AR) with Re_D varying from 220 to 700. They proposed that for very short bodies (AR < 7.5), the flow transition to three dimensionality is through mode-A and mode-B respectively, and mode-A instability dominates the flow. However for intermediate and long bodies (AR > 7.5), the flow

transition to three dimensionality is through mode-B first and then mode-A at higher Reynolds number, and mode-B instability plays a dominant role in the near wake dynamics. They reported a spanwise spacing (λ_z/D) of 3.5D for Mode-A and 2.2D for Mode-B. They also observed a third instability mode, mode-S with a saptio-temporal structure of mode-C, but with a spanwise spacing of the order one diameter (spacing similar to mode-B instability in circular cylinder flows). Further adding support to this argument, Sheard et al. [21] confirmed that the near wake flow of a bluff ring is dominated by sub-harmonic three dimensional instability mode-C. Sheard et al. [22] also demonstrated that transition to three dimensional flow in the near wake of a square cylinder with variation in incidence angles, mode-A instability or subharmonic mode-C instability dominated the flow structure. Carmo et al. [23] studied the flow around two cylinders in staggered arrangement showed that mode-C is also present along with mode-A and mode-B depending on the relative position of the cylinders.

From the literature it can be inferred that the transition to three dimensional flow and the corresponding instabilities (mode-A, mode-B, mode-C or mode-S) may switch the order of appearance and dominate the flow structure. From the literature, the existence of a preferred spanwise wavelength associated with streamwise vortices is not very clear. While some researchers indicate that spanwise wavelength is broadband [6, 20, 24], being imposed by the upstream conditions, others showed evidence of a preferred natural spanwise wavelength [9, 14, 15]. The preferred spanwise wavelength is rather scattered and are explained both by the presence of ribs or/and by the spanwise roll distortions. However it appears that the preferred spanwise wavelength is a function of flow configuration i.e. geometry [20, 21, 22, 23] and aspect ratio [20] of the wake generator, inflow conditions such as the Reynolds number and turbulence characteristics [9, 25], as well as function of the downstream distance [26].

Characterizing the near wake is challenging because of the wake decomposition into primary and secondary instabilities arising sequentially is only conceptual, and in many flows both may develop simultaneously. From modeling and flow control point of view, the minimum number of degrees of freedom (or modes) required to effectively describing the near wake and there by the dynamics is the question that needs attention. The POD objectively extracts a complete set of spatial eigenfunctions (i.e. modes) from the measured second-order cross-correlation matrix. The extracted POD modes serve as a set optimal basis functions for expansion of the flow. The resulting expansion is optimal in the sense that the convergence is more rapid than for any other possible basis. That is the projection of POD modes on velocity field is maximized. In general the extracted POD modes are closely related to coherent structure, although the exact relation is still debated. Lumley [28] noted that dominant POD modes represent the coherent structure only if it contains the dominant percentage of the fluctuating energy. Otherwise the POD modes may give an optimal basis function, but may have to do little with the physical shape of the underlying coherent structures.

Primary objective of this study is to characterize the coherent structures in the near wake region of a blunt trailing profiled body via the POD. We seek to experimentally extract the POD eigenfunctions and eigenvalues. Particular attention is focused to identify which three dimensional instability dominate the transition to turbulence. In the following section of this paper, we present the results of an experimental investigation of PLIF and PIV measurements aimed at characterizing the near wake flow topology and the unstable wavelengths associated with these instabilities.

2. EXPERIMENTAL SETUP

Facility and the Model

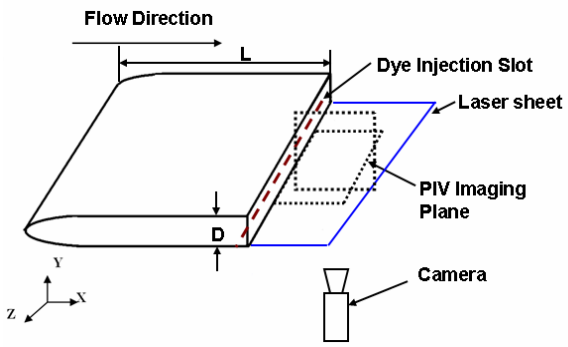

Figure 2. Flat plate model used for this investigation, along with schematic of the region in the near wake of the model imaged by the PIV system and flow visualization

All the measurements for this investigation are performed in the 0.61 m x 0.305 m cross section water tunnel facility at The Boundary Layer Wind Tunnel Laboratory. The facility is open return water tunnel producing a maximum free-stream velocity of 0.2 m/s. The water introduced into the water tunnel is passed through a settling chamber consisting of honeycomb and screens to break down large scale non-uniformities. The mean velocity profile varies with in 1% and the turbulence intensity is less than 1% in the test section.

For this study, the water tunnel was operated at a free stream velocity of $U_\infty = 0.02$ to $0.05\ m/s$, equivalent to Re_D varying from 250 to 550 at 15ºC. The model has a thickness of D = 0.0127m, a chord of 0.1587m (12.5D), and a total span of 0.6m (48D). Visualizations and measurements have been carried out over a 34D portion of the span, which is bounded by two transparent endplates. The endplates isolate the body from the effects of the boundary layers on the sidewalls of the tunnel, as well as the dye supply system tubing. The fluorescent dye is introduced to the flow through a thin spanwise slot on the lower surface of the body, located 1D upstream of the trailing edge. A horizontal light sheet is generated using an Nd-YAG laser with 532nm wavelength. The dye, which is a Rhodamine 6G solution, emits a fluorescent light with 560nm wavelength when

exposed to the laser. The 550nm color filter blocks the laser light reflections and allows the CCD camera to capture only the fluorescent light emitted by the dye. The images have been recorded using a capture rate of 15 frames per second with a camera resolution of 1200 x 1600 pixels. PLIF measurements were performed in XY, XZ planes.

The same system is used for the PIV measurements. The wake velocity field is determined from raw images using a cross-correlation 50% overlapping window of 32x32 pixels yielding 99 x 74 vectors with a spatial resolution of 1.83 mm (0.144D). A schematic of the location in the near wake where PIV measurements are performed relative to the flat plate model is shown in figure 2. A total of 3000 PIV images were acquired for the experiment. PIV measurements were carried out in XY and XZ (Y/D = 0: Shear layer) planes.

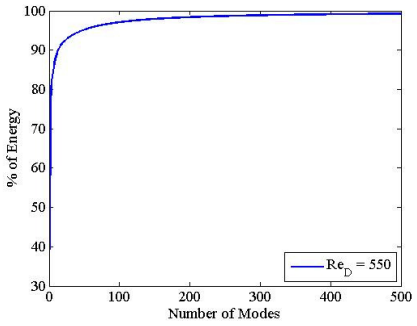

Figure 3. Cumulative convergence of relative energy in XY plane at Re_D = 550

4. PROPER ORTHOGONAL DECOMPOSITION

For this investigation, Proper Orthogonal Decomposition (POD) is used to study the near wake instabilities. POD analysis yields a set of Eigenvectors or POD modes (ϕ_i) that are optimal orthogonal basis functions. In this investigation, these POD modes are optimized for the kinetic energy and the combination of these POD modes provide information about the spatial structures of the investigated flow field. The Eigenvalues (λ_i) associated with each of these POD modes, represent the kinetic energy captured by the corresponding POD mode. Using these POD modes the instantaneous velocity field can be reconstructed [28] using

$$\bar{u}(\bar{x},t) = \sum_{n=1}^{N} a^n(t)\phi^n(\bar{x}) \qquad (1)$$

where $a_i(t)$ is the time varying coefficient for the ith POD mode (ϕ_i) at time t. These time varying coefficients are determined by projecting the instantaneous velocity field $\bar{u}(\bar{x},t)$ onto the POD modes.

When the number of grid points is much grater than the number of snapshots, it is appropriate to use the computationally more efficient method formulated by Sirovich [29]. The advantage of this formulation is that the dimension of the problem is given by the number of instantaneous fields or snapshots, where in the original formulation, the problem depends on the size of the physical grid times the number of components of the signal. For the present analysis, method of snapshots is implemented for U and V components combined in vector format. Figure 3 shows the cumulative converge of energy using snapshot POD in XY plane data.

5. PHASE AVERAGING

Measurements of phase-averaged quantities need a reference signal from which the phase of the flow is determined. Several choices are possible: Wlezien and Way [30] have used the velocity signal measured by the hotwire technique just above the boundary layer on the cylinder, near the separation line, and used Hilbert transform technique to measure the phase of the signal. Cantwell and Coles [31] used the pressure signal on the cylinder and used a phase locked loop (PLL) component to measure the phase of the signal.

However in the case of water tunnel experiments obtaining reference signal was difficult in our case. So extracting phase data from the available PIV data is explored here. The POD coefficients of the first two modes can be used to extract the phase of the vortex shedding instead of the pressure signal. Perrin et al. [32] demonstrated that temporal evolution of the POD coefficients is sinusoidal or quasi sinusoidal which can be used to extract the phase information from PIV data as

$$\varphi_{a_1-a_2} = \arctan\left(\frac{\sqrt{2\lambda_1}a_2}{\sqrt{2\lambda_2}a_1}\right) \qquad (2)$$

where λ_1 and λ_2 are the eigenvalues of the first two POD modes.

6. RESULTS AND DISCUSSION

Spanwise vortices

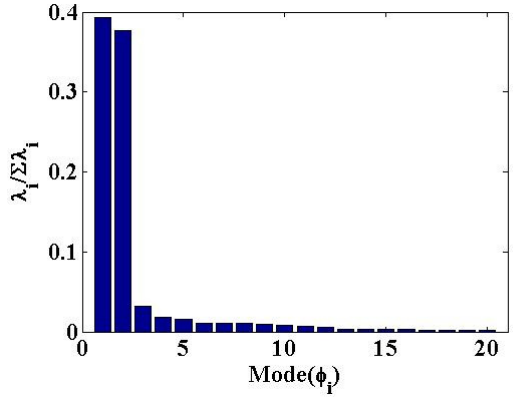

Figure 4. Relative energy captured by first twenty 2-D POD modes in XY plane at Re_D = 550

Figure 4 shows the relative energy captured by twenty 2D POD modes in XY plane. The relative energies indicate that the flow structure is dominated by the first two modes. These two modes represent the Karman vortices, which capture about 80% of the total relative energy in the flow. Figure 5(a) shows the Karman-Benard vortices captured by the PLIF experiments. Figure 5(b) shows the phase averaged streakline plots in the vertical plane, which captures the spanwise vortices as it would appear to an observer moving downstream at a velocity of $0.87U_\infty$. The mean velocities are reconstructed using the first two modes using equation 1. The streamwise distance (λ_X/D) of the spanwise vortices is found to be 4.8D

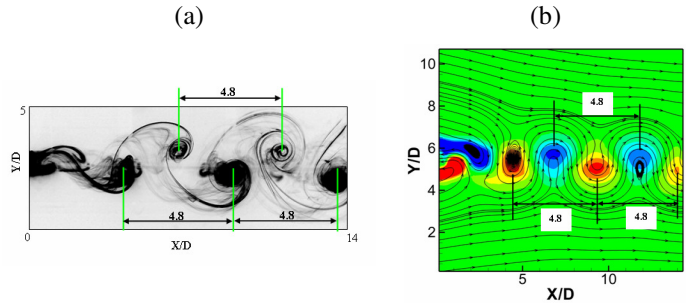

Figure 5. (a) PLIF Visualization (b) streakline plot along with vorticity contours of the first two POD modes at Re_D = 550.

Streamwise vortices

PLIF Visualization

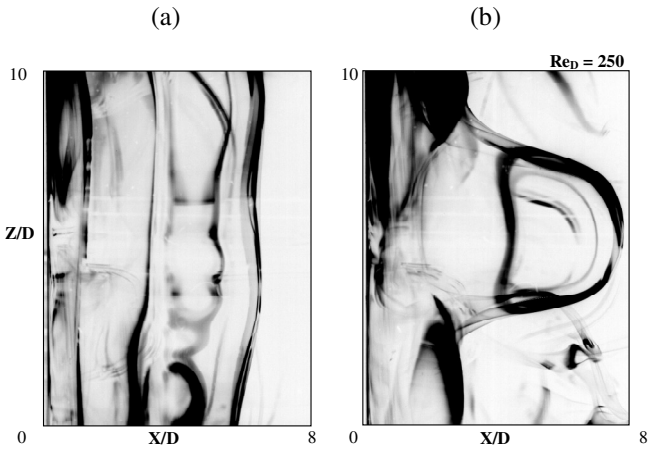

Figure 6. PLIF visualization at Re_D = 250 in XZ plane (a) Parallel vortex (b) Vortex dislocation

In the current experiment, to capture the flow phenomena in XZ plane, the dye was injected through a spanwise slot from the bottom surface of the flat plate. Hence the structure formed by the bottom shear layer appears darker than, on from the top shear layer. At the low Reynolds number (Re_D = 250) parallel shedding of the primary vortices is observed. The vortices shed regularly without showing much three dimensionality. The shedding of the primary vortices is parallel without any vortex loops, as shown in Figure 6(a). Vortex dislocation exists in the wake. These types of large scale vortex dislocations were observed by Williamson [33], Zhang et al. [14] in circular cylinder flows and Luo et al. [18] for square cylinder flows. Zhang et al. [14] referred to them as vortex adhesion modes. It appears that the dislocations observed in current flow configuration is mostly representative of two sided dislocations as defined by Williamson [33]. The vortex dislocations sustain for several shedding cycles before the flow is restored to parallel vortex shedding and the process repeats it self at this Reynolds number. As the Reynolds number increase beyond 350, the gradual inception of the streamwise vortices is observed. The initiation, growth and decay of the streamwise vortices is observed in Reynolds number range of 350-400.In this range they form intermittently and decay after few shedding cycles. Similar types of observation were made by Wu et al. [25] for circular cylinders in Re range of 150-175 and for square cylinder by Luo et al. [18] in the Re range of 150-175.

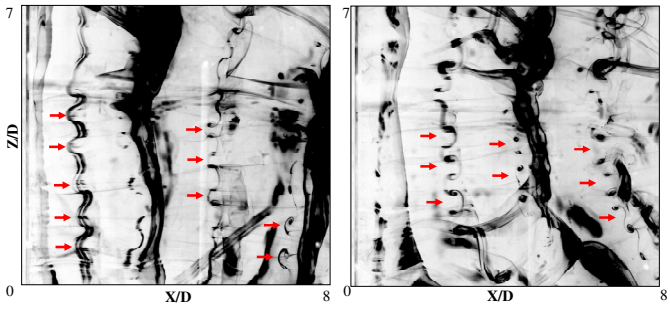

Figure 7. PLIF Visualization at in XZ plane at Re_D = 400

As the Reynolds number is increased beyond 400, the wake topology displays small scale streamwise vortices found in mode-B structure (Figure 7). The secondary vortices of the mode-B are simply connected over several shedding cycles are not associated with the severe distortion or reorientation of segments of Karman vortices. No vortex tongues are observed. Williamson [34] and Brede et al. [35] suggest that the secondary vortices of mode-B may have the origin in the separated shear layer in the near wake of the wake generator which could undergo stretching in the braid region connecting the initially formed Karman vortices. The spanwise spacing of the streamwise vortices is found to vary between 1.0D to 1.6D. This structure is observed in the Reynolds number range of 400 to 500.

Beyond Reynolds number 550, the wake topology displays two types of wake structures. In the very near wake, the wake topology display a mode-C structure and in the downstream wake (X/D>3), it display mode-A topology. Figure 8(a) shows the asymmetric pattern of the wavy structure indicating that mode-C instability is captured here. The structure display a uniform spanwise spacing as sinusoidal undulations in the near wake. The spanwise spacing of the streamwise vortices is found

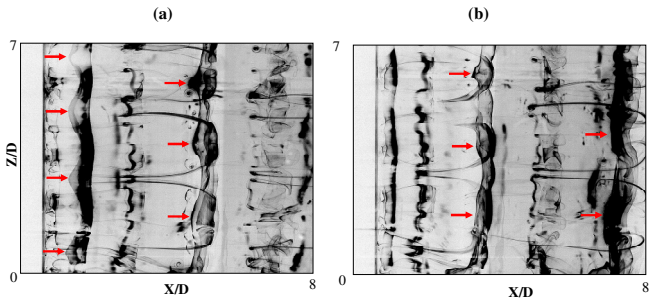

Figure 8. PLIF Visualization at in XZ plane at Re_D = 550

to vary between 2D to 2.7D in the very near wake. Figures 8(b) shows the appearance of mode-A instability in the downstream wake at the same Reynolds number of 550. This instability causes spanwise waviness that grows until a vortex loop is pulled out of the deforming primary vortices. These vortex loops are further stretched in braid shear region near the saddle point. When these vortex loops are pulled and stretched, the sides of the loop roll up to form streamwise vortex pair due to strain rate between the primary structures. It can be seen that that initial spanwise waviness in the primary vortex core was deformed by previous vortex loop, thus generating a series of self sustaining loops at the same spanwise position, as suggested by Wei and Smith [36]. The spanwise spacing of the streamwise vortices is found to vary between 2.8D to 3.6D beyond X/D > 3. The possible reason for the change in the near wake structure is given by Ryan et al. [20], who showed that perturbation streamwise vorticity in the newly formed vortices (Ryan et al. [20] : figure 10) in the top half of the vortex street has swapped sign for the profiled flat body as compared to the circular cylinder flow. This results in reversal of wake by half a cycle and the streamwise vorticity of opposite sign to dominate the near wake developing in the braid region leading to a different spatial structure at the corresponding downstream position. The other important observation is that the mode-C structure is dominant in the very near wake and is observed in the formation region of the near wake, whereas mode-A structure dominates the downstream wake development at the same Reynolds number.

Three wake instabilities are observed in the current flow configuration from PLIF visualization with a spanwise spacing varying between 1.0D to 1.6D, 2.0D to 2.7D and 2.8D to 3.6D. The larger wavelength structure clearly displays a topology of mode-A with a smaller spanwise spacing compared to cylinder flows of 4D to 5D. The smaller spanwise spacing structure in the current flow configuration displays a spanwise spacing larger than the mode-B structure in cylinder flows of 0.8D to 1.0D. Mode-C instability has a spanwise spacing similar to, as observed by Zhang et al. [14] (2D), Robichaux et al. [15] (2.8D) and Sheard et al. [21] (1.9D). Nevertheless Ryan et al. [20] proposed that larger spanwise spacing for mode-B structure of 2.2 D and smaller spanwise for mode-A structure of 3.2 D for a similar geometry used in the current experiments. They also reported that mode S structure with a spanwise spacing of 1D. Evidently from the PLIF visualization it is clear that the transition to three dimensionality through the traditional route of first transitioning to mode-A and then mode-B is not observed here. In fact the transition to three dimensionality is in the reverse order. First, a structure with small spanwise wavelength in the order of 1.2D to 1.6D is observed, followed by a larger wavelength structure with a spanwise wavelengths in the range of 2.0 to 2.7D for mode-C and 2.6 D to 3.6D for mode-A. However the debatable points still is whether mode-C or mode-A dominates the near wake transition to turbulence. In order to find some more answers we performed POD on PIV data obtained in the horizontal plane in the shear layer (Y/D = 0), to identify the dominant wake instability.

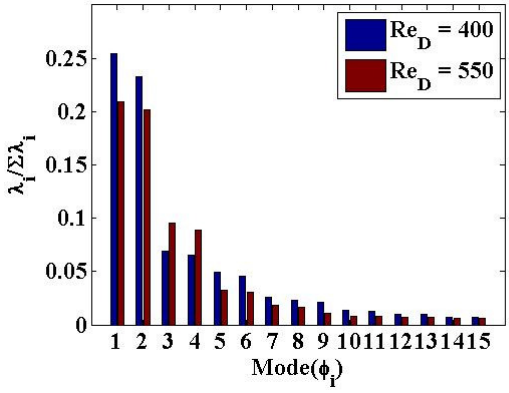

Figure 9. Relative energy captured by first fifteen 2-D POD modes in YZ plan at Re_D = 400 and 550

POD Analysis

Figure 9 shows the eigenvalues corresponding to the first 15 POD modes at Y/D = 0 (shear layer) at Re_D of 400 and 550. It clearly shows that significant relative energy is captured in the first 10 POD modes at Y/D = 0. It can be noted that the effect of the dominant coherent structure i.e. the Karman vortex is captured by the first two modes, as they show relatively high energy content compared to other modes. In order to identify

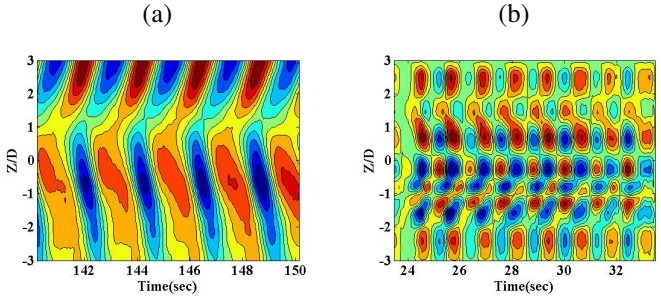

Figure 10. ω_y vorticity contours of (a) Combing POD modes 1 to 4 (b) Combining POD modes 5 and 10 at Re_D = 400

the underlying coherent structures, POD modes need to be combined [28].

Figure 10 shows the temporal and spatial evolution of ω_y vorticity contours using Taylor's hypothesis. Here only 10 seconds of data is shown. The actual data contains 200 seconds of data. Figure 10(a) shows the vorticity contours by combining the first four POD modes at Y/D = 0 for Re_D = 400. This clearly indicates that these modes represent the primary coherent structure i.e. the Karman-Benard vortices. Figure 10(b) shows the vorticity contours obtained by combining modes 5 to 8. These represent the streamwise vortices. As observed from the PLIF visualization (Figure 7), we understand that the streamwise vortices are simply connected over several shedding cycles, and are not associated with the severe distortion or reorientation of Karman vortices. The POD modes display the effect of the streamwise vortices as a sinusoidal oscillation shown in the schematic Figure 11. The spacing between the undulations is found to vary between 0.8D to 1.6D with an

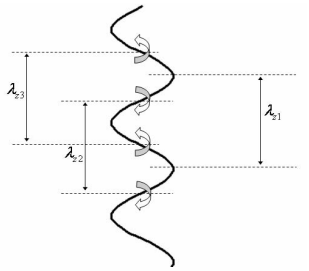

Figure 11. Schematic of the primary and secondary structures

average wavelength of 1.2D.

Figure 12(a) shows the vorticity contours by combining the first four POD modes at Y/D = 0 for Re_D = 550. This clearly indicates that these modes represent the primary coherent structure i.e. the Karman-Benard vortices. Figure 12(b) shows the vorticity contours obtained by combining modes 5 and 6. These represent the undulations caused by the streamwise vortices in the spanwise vortices, as shown in figure 11, in the very near wake (X/D < 3) of the mode-C topology. The spacing between the undulations is found to vary between 2.2D to 2.6D with an average wavelength of 2.4D. Figure 18(d) shows the vorticity contours obtained by combining modes 7 and 8. These represent the undulations caused by the streamwise vortices on the spanwise vortices in the near wake (X/D >3) of the mode-A topology. The spacing between the undulations is found to vary between 3.2D to 3.8D with an average wavelength of 3.5D. Figure 12(d) shows the vorticity contours obtained by combining modes 9 to 12. These modes display the small scale structure observed in the PLIF visualization. The interesting point to be noted is that these modes display finger like structures, without any influence of the Karman vortices. The topology of these vortices indicate a mode-B topology appearing for few shedding cycles Few interesting points to be noted here before we proceed further

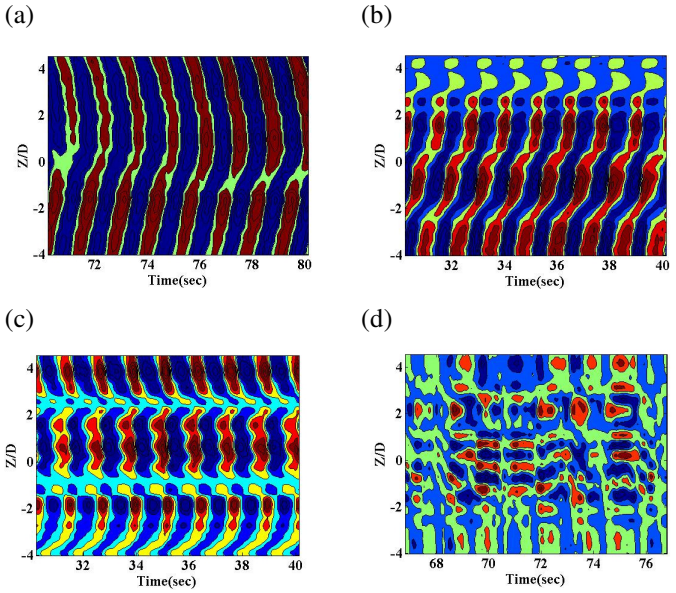

Figure 12. ω_y vorticity contours of (a) Combing POD modes 1 to 4 (b) Combining POD modes 5 and 6 (c) Combining POD modes 7 and 8 (d) Combining POD modes 9 to 12 at Re_D = 400

- Mode-A and mode-C instabilities are associated with the instability of the primary vortex core, as we observe the topologies of these instabilities as an effect on the primary instability in the POD modes
- Mode-B instability appears to be developing in the separated shear layer of the near wake.

The spanwise wavelengths of the instabilities observed in the current flow configuration are inline with the results from Ryan et al. [20], Dobre and Hangan [38] and El-Gammal and Hangan [39]. Ryan et al. [20] proposed that the unstable wavelength that is associated with similar aspect ratio geometry used in the current study is 2.2 based on numerical simulations at a Re_D of 500. Dobre and Hangan [38] proposed a spanwise wavelength of 2.4 for a square cylinder body at a Re_D of 22000. El-Gammal and Hangan [39] proposed a wavelength of 2.4 for airfoil geometry with a blunt diverging trailing edge at Re_D of 13000. We observed that near wake is dominated by Mode-C topology in the near wake and by mode-A topology as it convects downstream. Dobre and Hangan [38] proposed that a variant of mode-A topology dominated the intermediate wake for the square cylinder flow; where as Ryan et al. [20] and El-Gammal and Hangan [39] proposed that a Mode-B structure dominates the near wake development. The wavelength associated with mode-A structure in the current flow configuration i.e 3.5D matches with that proposed by Ryan et al. [20].

Conclusions

We have studied the development of secondary instabilities in the near wake of a profiled leading edge and blunt trailing edge flat plate body. Three instability modes (mode-A, mode-B and mode-C) are observed in the near wake transition to turbulent state. Mode-B instability undergoes transition at low Reynolds number, with the same spatio-temporal characteristics, but with a larger spanwise wavelength of 0.8 to 1.6D compared to 0.8 to 1.0D of circular cylinder flows. The transition Reynolds number is also much higher at 400 compared to circular cylinder flows of 188. The next transition in the flow is due to mode-C instability occurs with an average spanwise spacing of 2.4D at a Reynolds number of 550. However as this wake convects downstream, the instability display a mode-A topology with a spanwise spacing of 3.5D. Mode-B topology is also observed at this Reynolds number in higher POD modes indicating that all the three modes coexist at this Reynolds number, but is not the dominant instability that governs the wake transition. Another important observation is that the difference in the Reynolds numbers between transition of the instabilities for the current geometry is much higher i.e. from 400 for mode-B to 550 for mode-C and mode-A, as compared to the cylinder flows where the flows transitions at 188 and 230 for mode-A and mode-B, indicating that the wake transition mechanism is different for compact bodies and long bodies. Therefore it is proposed that the implicit assumption that wake of two dimensional bodies undergo transition to three-dimensional flow and eventually turbulence, through the same sequence of transition as observed in the circular cylinder flows is not universal. Other instability modes can play crucial role in the near wake development and the route to turbulence for vortex street depends on the geometric shape of the body.

REFERENCES

[1] Hussain, A.K.M.F., and Hayakawma, M., 1987. "Eduction of large-scale organized structure in a turbulent plane wake," *J. Fluid Mech.* **180**, pp 193- 229.

[2] Darekar, R.M. and Sherwin, S.J., 2001. "Flow past a square-section cylinder with wavy stagnation face," *Journal of Fluid Mechanics*, **426**, pp. 263-295.

[3] Tombazis, N. and Bearman, P. W., 1997. "A Study of three-dimensional aspects of vortex Shedding from a bluff body with a mild geometric disturbance," *Journal of Fluid Mechanics*, **330**, pp. 85-112.

[4] Dobre, A., Hangan, H. and Vickery, B.J., 2006. "Wake control based on spanwise sinusoidal perturbation," *AIAA Journal*, **44**(3), pp. 485-492.

[5] Lam, K., and F.Lin, Y., 2009. "Effects of wavelength and amplitude of a wavy cylinder in cross-flow at low Reynolds numbers," *J. Fluid Mech.* **620**, pp. 195- 220.

[6] Julien, S., Lasheras, J., and Chomaz, J., 2003. "Three-dimensional instability and vorticity patterns in the wake of a flat plate," *J. Fluid Mech.*, **479**, pp. 155-189.

[7] Unal, M., and Rockwell, D., 1988. "On vortex shedding from a cylinder. Part 1. The initial instability," *J. Fluid Mech.* **190**, pp. 491-512.

[8] Monkewitz, P., 1988. "The absolute and convective nature of instability in two-dimensional wakes at low Reynolds numbers," *Phys. Fluids A* **31**, pp. 999-1006 .

[9] Williamson, C. H. K., 1996. "Vortex dynamics in cylinder Wake," *Annu. Rev. Fluid Mech.*, **28**, pp. 477-539.

[10] Hammache, M., and Gharib, M., 1991. "An experimental study of the parallel and oblique vortex shedding from circular cylinders," *J. Fluid Mech.* **232**, pp. 567-590.

[11] Eisenlohr, H., and Eckelmann, H., 1989. "Vortex splitting and its consequences in the vortex street of cylinders at low Reynolds number," *Phys. Fluids A* **1**, pp. 189-192.

[12] Barkley, D., and Henderson, R.D., 1996. "Three-dimensional Floquet stability analysis of the wake of a circular cylinder," *J. Fluid Mech.* **322**, pp. 215-241.

[13] Prasad, A., and Williamson, C.H.K., 1997. "The instability of the shear layer separating from a bluff body," *J. Fluid Mech.* **333**, pp. 375-402.

[14] Zhang, H., Fey, U., Noack, B.R., Konig, M., and Eckelmann, H., 1995. "On the transition of the cylinder wake," *Phys. Fluids* **7** (4), pp. 779-794.

[15] Robichaux, J., Balachandar, S. and Vanka, S. P., 1999. "Three-dimensional floquet instability of the wake of square cylinder," *Physics of Fluids*, **11**(3), pp. 560–578.

[16] Blackburn, H.M., and Lopez, J.M., 2003. "On three-dimensional quasi-periodic Floquet instabilities of two-dimensional bluff body wakes," *Phys. Fluids* **15** (8), L57-L60.

[17] Sohankar, A., Norberg, C., and Davidson, L., 1999. "Simulation of three-dimensional flow around a square cylinder at moderate Reynolds numbers," *Phys. Fluids* **11** (2), pp. 288-306.

[18] Luo, S.C., Chew, Y.T., and Ng, Y.T., 2003. "Characteristics of square cylinder wake transition flows," *Phys. Fluids* **15** (9), pp. 2549-2559.

[19] Luo, S.C., Tong, X.H., and Khoo, B.C., 2007. "Transition phenomena in the wake of a square cylinder." *J. Fluids Struct.* **23**, pp. 227-248.

[20] Ryan, K., Thompson, M.C., Hourigan, K., 2005. "Three-dimensional transition in the wake of elongated bluff bodies", *J. Fluid Mech.* **538**, pp. 1-29.

[21] Sheard, G.J., Thompson, M.C., Hourigan, K., and Leweke, T., 2005. "The evolution of a subharmonic mode in a vortex street," *J. Fluid Mech.* **534**, pp. 23- 28.

[22] Sheard, G.J., Fitzgerald, M.J., and Ryan, K., 1996. "Cylinders with square cross-section: wake instabilities with incidence angle variation," *J. Fluid Mech.* **630**, pp. 43-69.

[23] Carmo, B. S., Sherwin, S.J., Bearman, P.W., and Willden, R.H.J., 2008. "Wake transition in the flow around two circular cylinders in staggered arrangements," *J. Fluid Mech.* **597**, pp. 1-29.

[24] Meiburg, E., and Lasheras, J.C., 1988. "Experimental and Numerical Investigation of the Three-Dimensional Transition in Plane Wakes," *J. Fluid Mech.* **190**, pp. 1-37.

[25] Wu, J., Sheridan, J., Welsh, M.C., and Hourigan, K., 1996. "Three-dimensional vortex structures in a cylinder wake," *J. Fluid Mech.* **312**, pp. 201-222.

[26] Mansy, H., Yang, P.M., and Williams, D., 1994. "Quantitative measurements of three-dimensional structures in the wake of a circular cylinder," *J. Fluid Mech.* **270**, pp. 227-296.

[27] Lumley, J., 1981. "Coherent structures in turbulence," In Transition and Turbulence (ed R.E. Meyer), pp. 215-242.

[28] Holmes, P., Lumley, J. L., and Berkooz, G., 1996. *Turbulence, Coherent Structures, Dynamical System and Symmetry*, Cambridge, 1st ed.

[29] Sirovich, L., 1987. "Turbulence and the Dynamics of Coherent Structures," Parts 1, 2 and 3, *Quarterly of Applied Mathematics*, **45**(3), pp. 561-590.

[30] Wlezien, R.W. and Way, J.L., 1979. "Techniques for the experimental investigation of the near wake of a circular cylinder," *AIAA Journal*, **17**(6), pp.563-570.

[31] Cantwell, B. and Coles, D., 1983. "An experimental study of entrainment and transport in the turbulent near wake of a circular cylinder," *Journal of Fluid Mechanics*, **136**, pp. 321-374.

[32] Perrin, R., Braza, M., Cid, E., Cazin, S., Barthet, A., Sevrain, A., Mockett, C., and Thiele, F., 2007. "Obtaining phase averaged turbulence properties in the near wake of a circular cylinder at high Reynolds number using POD," *Exp. in Fluids*, **43**, pp. 341-355.

[33] Williamson, C.H.K., 1992. "The natural and forced formation of spot-like 'vortex dislocations' in the transition of a wake," *J. Fluid Mech.* **243**, pp. 393-441.

[34] Williamson, C.H.K., 1996. "Three-dimensional wake transition," *J. Fluid Mech.* **328**, pp. 345-407.

[35] Brede, M., Eckelmann, H., and Rockwell, D., 1996. "On Secondary Vortices in the Cylinder Wake," *Phys. Fluids* **8** (8), pp. 2117-2124 .

[36] Wei, T., Smith, C.R., 1986. "Secondary vortices in the wake of circular cylinders," *J. Fluid Mech*. **169**, pp. 513-533.

[38] Dobre, A., and Hangan, H., 2004. "Investigation of the three-dimensional intermediate wake topology for a square cylinder at high Reynolds number," *Exp. in Fluids*, **37**, pp. 518-530.

[39] El-Gammal, M. and Hangan, H., 2008. "Three-dimensional wake dynamics of a blunt and divergent trailing edge airfoil," *Exp. in Fluids*, **44**, pp. 705-717.